

Effect of Ca and P Ion Concentrations on the Structural and Corrosion Properties of Biomimetic Ca-P Coatings on ZK60 Magnesium Alloy

Caiwen Ou², Wei Lu^{1,*}, Zailei Zhan¹, Ping Huang¹, Pengfei Yan¹, Biao Yan¹ and Minsheng Chen^{2,*}

¹ School of Materials Science and Engineering, Shanghai Key Lab. of D&A for Metal-Functional Materials, Tongji University, Shanghai 200092, China

² Southern Medical University, No.1023, Shatai Nan Road, Guangzhou City, Guangzhou 510515, China

*E-mail: gzminsheng@vip.163.com; weilu@tongji.edu.cn

Received: 9 May 2013 / Accepted: 12 June 2013 / Published: 1 July 2013

Magnesium and its alloys have attracted more and more attentions due to their potential applications in biodegradable implants. But the applications are limited by high corrosion rate of magnesium. In this paper, CaP coatings were fabricated on the ZK60 magnesium alloys by a biomimetic method. The revised SBF solutions with ion concentration of Ca and P elements varied from 0.5 to 2 times of that of standard r-SBF are used. The coatings were composed of amorphous and poorly crystallized CaP phases with globule structure. SEM images show that crack density and size decrease with increasing Ca/P ion concentration. Electrochemical corrosion and in vitro immersion were conducted to evaluate the corrosion resistance. The corrosion resistance of the coated samples was greatly improved comparing with that of the uncoated sample. For the samples fabricated at different Ca and P ion concentration, the sample coated from the 2×r-SBF solution with has the best corrosion resistance.

Keywords: magnesium alloy; Ca-P coating; biomimetic deposition; corrosion;

1. INTRODUCTION

Materials like titanium and its alloys, steel, and cobalt–chromium alloys are widely used as implant materials in load-bearing devices for the repair and replacement of bone tissues [1,2]. Although these metals have proven to be effective in providing the required mechanical support during the healing process, stress shielding can occur resulting in decreased implant long-term stability. Furthermore, there exist problems of metal ions release [2,3], which lead to physiological inflammatory effects and the necessity of a second surgical procedure to remove implants [1-5]. To

overcome the need for this second surgery, biodegradable implants have been proposed. These materials would provide the necessary stability in the initial stages of healing and would gradually be replaced by bone as they degraded

Magnesium and its alloys have been suggested as a revolutionary metallic biomaterial for the design of orthopedic devices. They are more suitable for load-bearing applications due to their excellent mechanical properties and characteristics, i.e. the specific density (1.74–2 g/cm³) and Young's modulus (41–45 GPa) of magnesium are close to those (1.8–2.1 g/cm³, 3–20 GPa) of human bone [1,6,7]. Some researchers [8] reported that magnesium has antibacterial properties. The greatest novelty Mg provides is its ability to degrade within a physiological environment removing the necessity for implant removal at a later stage. Biodegradable implants can be gradually dissolved, absorbed and excreted in a biological environment owing to their corrosion. Thus, magnesium alloys combine biocompatibility, biodegradation and mechanical properties which are similar to natural bone which makes them promising materials for biodegradable implants.

Whilst the corrosion of Mg provides a novel advantage over other metallic materials, the adaptation of this material for orthopedic purposes requires corrosion rates to be closely controlled to match bone healing. Recently, the corrosion properties of Mg and its alloys have been investigated extensively [9–16]. The main problem for magnesium and its alloys is that their corrosion rate in the physiological environment with high chloride concentration is too high due to their reactive properties. Thereby, they lose their mechanical integrity long before the expected service life [1,2]. Therefore, the main research activities are focused on how to protect magnesium from fast corrosion and improve corrosion resistance of Mg alloys [17–26]. To date, still a limited number of studies on the use of Mg as a biodegradable material have been conducted (reviewed in [1]), with many open questions remaining.

To tailor the degradation rate of the Mg-based implant for the specific biomedical application, a lots of studies have been performed for the purpose of reducing the corrosion rate of Mg, including alloying [17–19], processing [20,21] and protective coating [22–26] Previous research has investigated the use of hydroxyapatite (HA) coatings on titanium orthopedic implants with success in regards to increased biocompatibility and decreased wear of the implant.[27,28] Furthermore, hydroxyapatite, the major composition of bone, have demonstrated high biocompatibility, osteoconductivity and non-toxicity in an in vivo environment.[27–29] Such evidence advocates that bioactive HA coating on Mg alloys might be an effective way to solve this problem. There are various techniques for HA coating deposition onto Mg substrates: chemical deposition, electrodeposition, hydrothermal treatment and alkali-heat treatment.[29,30] Though many methods for fabricating HA coatings are available, the biomimetic method [31–34] offers the advantages of a simple, low temperature, non-toxic and non line-of-sight process. The technique is relatively simple to set up and perform, and is a cost-effective way of creating homogeneous coatings on several samples simultaneously and allows for complex shapes to be coated. The biomimetic coating process uses only ions found in the body fluids to create safe, biocompatible coatings with properties similar to natural bone.

The main mineral component of bone is calcium deficient carbonate hydroxyapatite. Calcium phosphate coatings have been shown to improve the biocompatibility of metallic implants and to increase bone growth at the site of implantation. In particular, biomimetically deposited coatings have

received recent attention because of their excellent biocompatibility and ability to promote osseointegration.[31-34] The biomimetic approach is a solution technique that involves immersing the substrate material in SBF at low (ambient to physiological) temperatures. This technique has been successfully used to apply calcium phosphate coatings onto various substrates. [27,28] The technique is relatively simple to set up and perform, and is a cost-effective way of creating homogeneous coatings on several samples simultaneously and allows for complex shapes to be coated. The biomimetic coating process uses only ions found in the body fluids to create safe, biocompatible coatings with properties similar to natural bone. The composition of the coating bath and the chemistry of the implant surface have both been shown to play a key role in the nucleation and growth of calcium phosphate coatings from SBF.

Zinc is recognized as a highly essential element for humans. In zinc deficiency, nearly all the physiological functions are strongly perturbed. Zirconium possesses a set of suitable properties for orthopedic applications such as low specific weight, high corrosion resistance, and biocompatibility. Based on the above considerations, ZK60 magnesium alloy (Mg-5.5wt%Zn-0.5wt%Zr) was chosen in our studies. In this study, biomimetic techniques used for HA-based CaP coating deposition are carried out in revised simulated body fluids (r-SBF), where CaP phases are precipitated out of solution and 'grown' on the ZK60 substrate. The ion concentration of Ca and P elements is varied from 0.5 to 2 times of that of standard r-SBF in order to refine fabricating protocols of CaP coatings. The microstructure and composition of the biomimetic CaP coatings were characterized, and the degradation properties were also investigated.

2. EXPERIMENTAL

2.1 Sample Pretreatment

The magnesium alloy used in this study was ZK60 alloy, with the major alloying elements of approximately 5.5wt% Zn and 0.5wt% Zr. It was cut into rectangular samples with a size of $10 \times 10 \times 5 \text{ mm}^3$. These samples were ground with SiC papers up to 800#, rinsed ultrasonically in ethanol and then air dried. The dried samples were etched in phosphoric acid solution at 55°C , followed by neutralization in NaOH solution. Samples were then rinsed with distilled water and air dried.

Subsequent pretreatment procedures include alkaline aging in a 200 g/L sodium hydroxide solution (Aldrich) followed by heat treatment for 24 h at 140°C . Alkaline aging was used to increase the surface concentration of hydroxyl groups. This has been shown to be effective in inducing calcium phosphate deposition from aqueous solutions on other materials such as titanium and stainless steel.

2.2 Biomimetic CaP Coating

In this study, the Mg samples prepared earlier were applied with a layer of biomimetic Ca-P coating using a revised SBF. The ion concentrations of SBF and the revised SBF are listed in Table 1. These Ca and P concentrations were chosen to maintain the stoichiometric ratio of Ca/P in hydroxyapatite, 1.67:1, and several times as high as those of the SBF respectively. The pH of the

revised solution was adjusted to 6, using either hydrochloric acid or sodium hydroxide as required. The pre-treated Mg samples were immersed in the revised SBF for 3 days at ambient temperature. The samples were then removed from the solution, rinsed with deionized water, and dried in air.

Table 1. Composition of SBF and revised SBF solution

components	concentration				
	Revised SBF(g/L)	0.5×R-SBF(g/L)	1.5×R-SBF(g/L)	2×R-SBF(g/L)	SBF(g/L)
CaCl ₂	0.333	0.167	0.500	0.666	0.1397
MgSO ₄	0.09767	0.09767	0.09767	0.09767	0.09767
KCl	0.4	0.4	0.4	0.4	0.4
KH ₂ PO ₄	0.06	0.06	0.06	0.06	0.06
NaHCO ₃	0.335	0.335	0.335	0.335	0.355
NaCl	8.0	8.0	8.0	8.0	8.0
Na ₂ HPO ₄ ·12H ₂ O	0.256	0.128	0.384	0.512	0.1206
D-Glucose	1.0	1.0	1.0	1.0	1.0

2.3 Surface Characterization

The crystallographic structure and chemical compositions of the coatings were examined using X-ray Diffraction (XRD) and energy dispersive spectroscopy (EDS), respectively. To study the morphology, coated samples were analyzed with a field emission scanning electron microscope (FE-SEM).

2.4 Electrochemical Measurements

Corrosion behavior of the samples was studied by electrochemical tests (Tafel Plot) with an electrochemical work station. The experiments were performed in the SBF solution (listed in Table 1) with a pH value of 7.4 at 37 °C. A three electrode set-up with a saturated calomel reference and a platinum counter electrode was used. The area of the samples for working electrode was 10×10mm². Prior to characterization, the samples were immersed in the solution for 20 min to establish the open circuit potential.

2.5 Immersion Tests

Immersion tests were carried out in SBF solution. The pH value was adjusted to 7.4 ± 0.1 and the temperature was kept at 37 ± 0.5 °C using a water bath. The samples were immersed into 120 ml SBF solution for 8 days, respectively. The pH value of the solution and the samples' mass were

recorded during the immersion every 24h, with a blank SBF solution as control group. The SEM characterizations were performed before and after immersion tests.

3. RESULTS AND DISCUSSION

Acid etching is a common pretreatment in preparation for surface coating. Acid etching of magnesium alloys is believed to remove the gross scale that is produced during the manufacturing process and to replace the native oxide layer with a more passive oxide layer. Figure 1 shows SEM images of a magnesium alloy sheet that has been solvent degreased [Fig. 1(a)] and a sample that has been etched in phosphoric acid [Fig. 1(b)]. It is clear from these images that prior to acid etching the sample surface have a non-uniform morphology with visible pits, whereas the acid-etched sample is much more homogeneous. To obtain coatings with minimum porosity and maximum adhesion a uniform surface is desirable.

Acid etching also results in significant changes in the surface chemistry of the magnesium alloy sheet. Following the acid etching step the samples are neutralized in a solution of sodium hydroxide. It is likely that the magnesium hydroxide forms at this stage. In fact, the formation of magnesium phosphate films during etching in phosphoric acid has been previously observed. The following reactions have been proposed for magnesium alloys with acidic phosphate solutions:

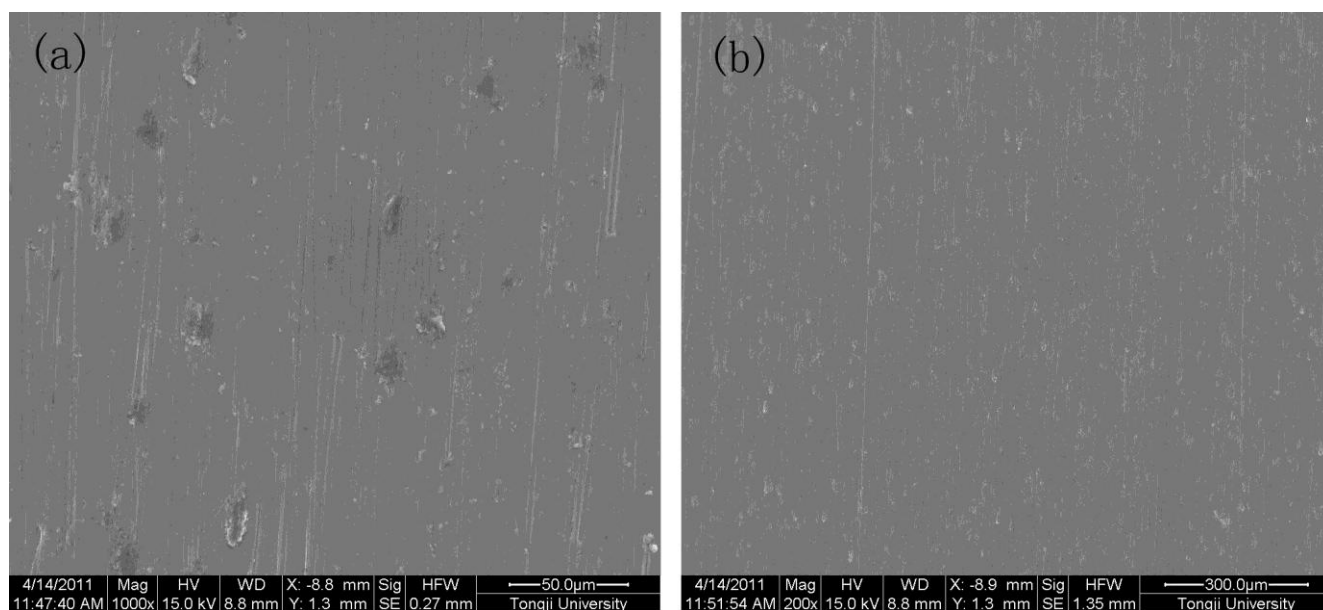
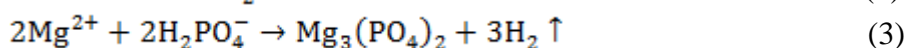


Figure 1. SEM images of a magnesium alloy sheet. (a) solvent degreased; (b) etched in phosphoric acid

In the first reaction, anodic dissolution of magnesium occurs because of its instability at pH values less than 11, and this is coupled with the reduction of hydrogen (reaction 2). Indeed, hydrogen bubbles were observed during etching of our samples. Finally, magnesium phosphate precipitates onto the surface of the alloy because of its low solubility.

3.1 Characterization of as-prepared CaP coatings

Figure.2 shows the XRD patterns of biomimetic CaP coatings fabricated with different ion concentration. It can be seen that there is a broad peak at $2\theta=30^\circ$ and the other peaks are relatively weak in the XRD pattern of all the samples. This indicates that the main part of the CaP coating is a poorly crystallized or amorphous Ca-P phase. A peak at $2\theta=32^\circ$ was observed in the XRD patterns, corresponding to overlapping of the (211) and (112) diffraction planes and indicative of a bone-like crystalline HA phase. At low ion concentration (0.5 and $1\times r$ -SBF), the peak intensity at $2\theta=32^\circ$ is very weak, indicating a poorly crystalline HA phase. With increasing ion concentration, the intensity of peak at $2\theta=32^\circ$ increases, indicating a better crystalline of HA phase. For all the samples, the FWHM (Full Width at Half Maximum) of the broad peaks decrease while the intensity of that increases with increasing ion concentration. In addition, the diffraction peaks from $Mg(OH)_2$ phase were clearly observed at $2\theta=19^\circ$ and 38° for the sample fabricated at ion concentration of $1\times r$ -SBF. Further increasing the ion concentration ($1.5\times r$ -SBF), the peak intensity of $Mg(OH)_2$ phase decreases and the diffraction peak of $Mg(OH)_2$ phase disappear evenly when the ion concentration was increased to $2\times R$ -SBF. It can be suggested that the crystallinity of HA phase increases with increasing ion concentration in current study.

In present study, the CaP coatings deposited on ZK60 substrate using r-SBF solutions with different Ca/P ion concentration were characterized mainly as amorphous CaP (ACP) phase by XRD, which is in accordance with literature which demonstrated the ability of depositing ACP on titanium substrate [27, 35]. Precipitation of various phases of CaP from solution involves the formation of an ACP as the initial phase prior to hydrolysis and conversion to other crystalline phases.[36] The presence of crystal growth inhibitors Mg^{2+} and HCO_3^- in the r-SBF solution inhibits the formation of a crystalline CaP phase and promotes the formation of ACP. Interestingly, when the substrates were coated with r-SBF solution with high Ca/P ion concentrations, the conversion of the ACP phase to poorly crystalline HA phase are observed from the XRD patterns. According to theoretical models based on classical crystallization theory, r-SBF solutions containing high concentrations of Ca^{2+} and PO_4^{3-} favor nucleation of HA compared to both DCPD and OCP. [37]. SEM images showing the morphology of the CaP coatings as a function of ion concentration in the coating bath are shown in Fig.3. SEM observation reveals the differences between the morphology of the CaP coatings formed at different Ca/P ion concentration. From Fig.3 (a), it can be seen that the CaP coating deposited at $0.5\times r$ -SBF solution is composed of globules with a diameter of about $1\sim 5\mu m$, and a lot of globules stacked so closely that it showed dense cluster structure on the surface, as seen from the high magnification ($\times 10000$) SEM images which are not shown here. Although the final coating covered the substrate more or less uniformly on the macro scale, cracks and defects were observed in the coatings from Fig.3

(a). For the coating deposited from the 1×r-SBF solution, it can be observed from Fig.3 (b) that the morphology of the coating is still composed globules with dense-cluster structure. Also, cracks and defects are clearly observed in this sample.

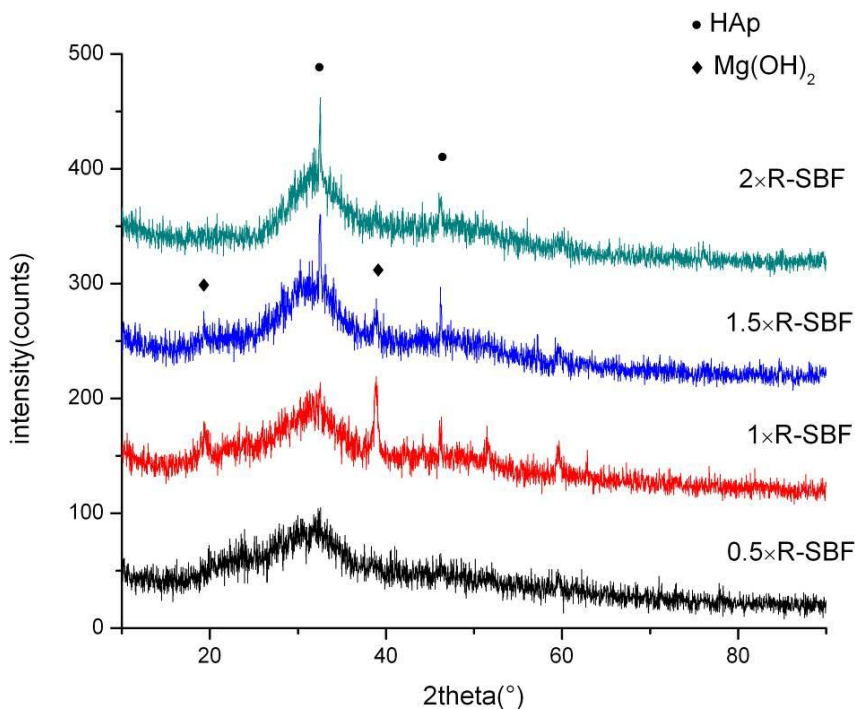


Figure 2. XRD patterns of coating powders in solutions with different Ca/P ratio

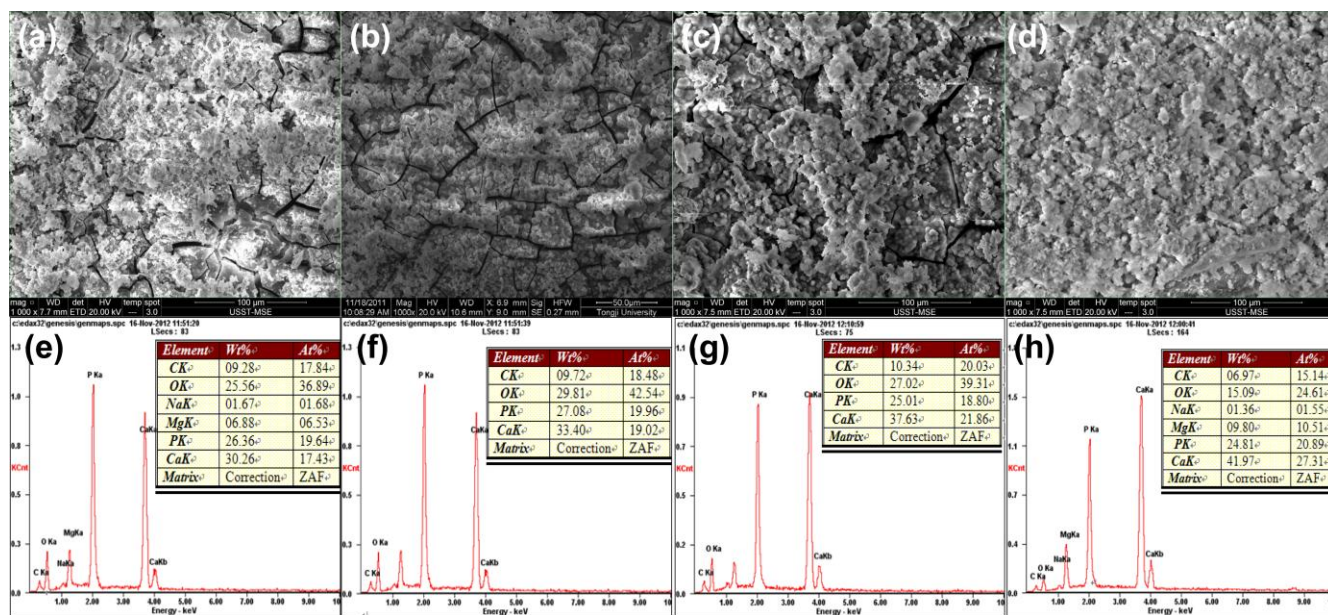


Figure 3. SEM morphologies and corresponding EDS patterns of coated samples. 0.5×R-SBF: (a)/(e) ; 1×R-SBF: (b)/(f); 1.5×R-SBF: (c)/(g); 2×R-SBF: (d)/(h)

Fig.3 (c) depicts the coating morphology of the sample deposited at $1.5\times r$ -SBF solution. The coating seems dense compared with the coatings precipitated at low Ca/P ion concentration. A similar globule-like morphology was observed in this sample. Interestingly, the coating is composed of two layers: outer layer and inner layer, as shown in Fig.3 (c). It can be observed from SEM image that the inner layer is dense while the outer layer is loose. Also, the cracks and defects are less. When the Ca/P ion concentration is increased to $2\times r$ -SBF solution, the outer layer in the CaP coating becomes dense and covers all the surface of substrate, as seen from Fig.3 (d). In addition, there is no cracks in the CaP coating can be observed from Fig.2 (d). Only pores were observed among these CaP clusters in Fig.2 (d). From SEM observation, crack density and size was found to decrease with increasing Ca/P ion concentration.

The compositions of the coatings deposited from the revised SBF solution with different ion concentration in the coating bath were examined by EDS, as shown in Fig.3 (e)~(h). The main elements detected on the surface of the coatings were Ca, P, C, and O indicating that CaP phase was present in the coating. Na and Mg were also detected in the coatings but the content is less. EDS analysis of the various coatings revealed that Ca/P atomic ratio was found to be around 0.89, 0.95, 1.16 and 1.31 for coatings deposited at Ca/P ion concentration of $0.5\times r$ -SBF, $1\times r$ -SBF, $1.5\times r$ -SBF, $2\times r$ -SBF, respectively, as shown in Fig.3. The Ca/P ratios of all the coatings are below that of the stoichiometric HAp (1.67). This result indicates that our hydroxyapatite coating is calcium-deficient. This is due to substitutions in the lattice. Calcium phosphate compounds can be substituted with different ions. In the HA lattice, calcium can be replaced by small amounts of magnesium and sodium, and phosphates can be replaced by carbonate ions [27]. During the biomimetic depositing process, these ions are incorporated into the coating. It is also known that there is a significant amount of magnesium incorporated into coatings which makes calcium magnesium hydroxyapatite the mostly like phase present due to the revised SBF solution and the corrosion of the substrate during the coating process. This is mostly due to the presence of Mg^{2+} and Cl^- ions in solution. In fact, it has been previously observed that the substitution of magnesium ions into the crystal structure of hydroxyapatite significantly decreases the crystallinity of the materials.[27] Substitution and interstitial Mg in the lattice affect the growth of the CaP crystal structure [38, 39]. EDX results confirmed minor amounts of Mg in all coatings. The subsequent dissolution and release of Mg^{2+} , as well as the initial Mg^{2+} concentration in solution, would have an influence on coating topography, since the presence of Mg^{2+} in solution is capable of reducing the surface roughness and producing apatite coatings exhibiting finer surface structures. [40] With increasing Ca/P ion concentration, the Ca/P atomic ratio in the coatings increases due to the reduction of lattice substitution of Mg and Na. This indicates that higher Ca/P ion concentration in the r-SBF solution results in higher Ca content in CaP phase in CaP coatings.

3.2 Electrochemical test in SBF

The potential dynamic polarization curves (PDP curves) obtained for CaP-coated and uncoated ZK61 alloy samples in SBF solution at $37^{\circ}C$ were plotted based on the electrochemical characterizations, as shown in Fig.4. Tafel-type analysis was performed on the linear regions of the

plot, using the Tafel slopes from between 50 and 250mV away from the corrosion potential, to provide an approximation of the corrosion current density. The corrosion potential (E_{corr}) was determined according to Tafel extrapolation and shown in Table.2. Generally, a material that has a higher corrosion potential will have a lower degradation rate. The initial corrosion potential (E_{corr}) of the CaP-coated Mg alloy samples were all higher than the uncoated alloy sample (-1.53V) and increase from 1.42 V to 1.24 V with increasing Ca/P ion concentration (0.5×r-SBF to 2×r-SBF), as shown in Table 2. The PDP tests showed that the biomimetic coating had a lower corrosion current density (as shown in Table.2) than the uncoated ZK60 alloy and corresponding higher polarization resistance. The lower current density was due to the smaller portion of exposed area to the solution. Thus, there was a decrease in anodic reaction rate (the corrosion rate). The coating decreases the available surface area susceptible to corrosion. The corrosive solution cannot attack the magnesium where it is protected by the CaP coating. This matched with the immersion testing results that the initial degradation rate of the CaP-coated samples was lower than the uncoated ones. From the results of electrochemical testing analysis, it is obvious that the Ca-P coating could improve effectively corrosion resistance of the ZK60 alloy in the SBF solution. The improvement in corrosion resistance will greatly reduce the initial biodegradation rate of the implants, and is essential for maintaining the implant’s mechanical strength in the bone reunion period. Thus ZK60 alloy coated with the Ca-P coating prepared in this study is a promising candidate for biodegradable orthopedic implant.

Table 2. Corrosion parameters obtained from electrochemical analysis

Samples	E _{corr} (V)	I _{corr} (A)
uncoated	-1.531	1.768e-004
0.5×R-SBF	-1.420	2.429e-006
1×R-SBF	-1.390	9.154e-007
1.5×R-SBF	-1.357	5.455e-006
2×R-SBF	-1.236	5.571e-007

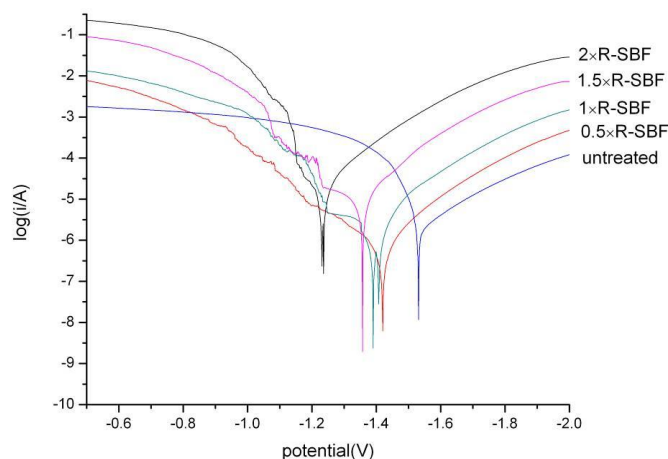


Figure 4. Tafel plot of the samples in SBF solution

3.3 Immersion test

To examine the long-term corrosion behavior, the in vitro corrosion behavior of the CaP-coated and uncoated ZK60 alloy samples in SBF were monitored. Fig.5 shows the relationship of sample weight versus immersion time. It was observed that the weight of coated samples do not change much and keep almost constant (there are a little bit increase) with increasing immersion time while that of uncoated sample decreases significantly. The weight change of the samples immersed in SBF solution was a result of the following three processes: (1) the corrosion of magnesium, (2) the precipitation of CaP coating, and (3) the dissolution of CaP coating. The corrosion of magnesium occurred for all the samples, but their corrosion rates were significantly different owing to varied surface coatings applied to the substrate, including no coating and coating at different ion concentrations. Besides the corrosion of magnesium, CaP precipitation and dissolution were two processes continuously occurred during the immersion in SBF solution. As the CaP coating formed was poorly crystalline or amorphous (Fig.2), it could dissolve in a physiological solution at a body temperature. It can be proposed that the CaP coating underwent a dynamic process of precipitation and dissolution during the immersion test. For the samples with a CaP coating, there was a small increase in the weight of the samples after immersion in SBF solution for 8 days. This indicates that more CaP phase was formed during the soaking in SBF solution, where the CaP precipitation process predominated over the dissolution process.

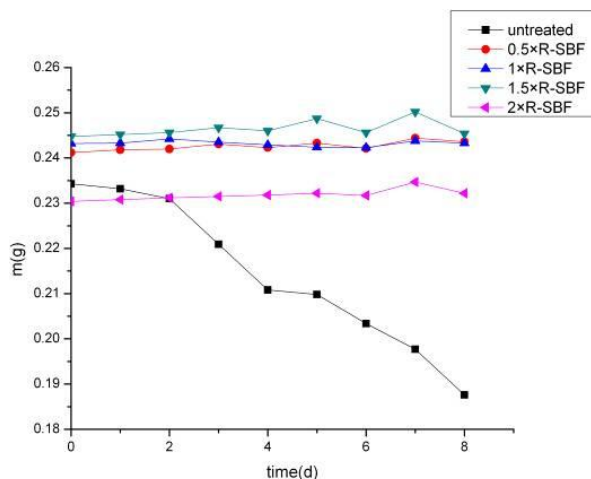


Figure 5. Relationship of sample weight versus immersion time

The pH values of the SBF were monitored every day during the sample immersion. Fig.6 shows the variation of the pH value of SBF solution at different immersion time. The corrosion rate of Mg alloys during the early stages of implantation would play a critical role in the initial surrounding tissue response. If the initial degradation of Mg-based implants was too rapid, osteolysis would occur, thus adversely affecting bone tissue regeneration.[41] Therefore, it was critical to control and decrease the initial degradation rate. From Fig.6, it can be seen that there is an increase in pH value for all the samples with increasing time. At the first day, the pH value increases sharply for all the samples because of the increase of OH^- concentration caused by the release of Mg^{2+} [42]. The pH for the

uncoated sample increases from 7.4 to 9 while the pH of coated samples increase only about 0.6 (reach to 8). After 2 days' immersion, the pH changes for all samples slow down. It is clear that the pH change for the uncoated sample was the highest and the pH value reaches to about 10.2 while the pH values of the solution immersed with CaP coated samples are around 8.0, which is much lower than that of uncoated samples. Therefore, it can be concluded that the samples coated with CaP have a better corrosion resistance than uncoated sample.

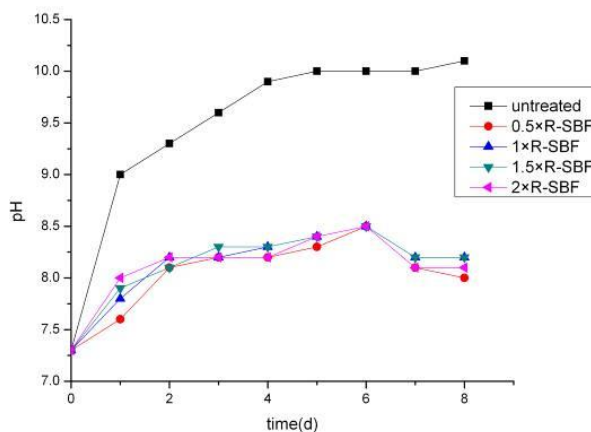


Figure 6. Variation of the pH value of SBF solution at different immersion time

4. CONCLUSIONS

In summary, Ca-P coating was successfully prepared on the ZK60 magnesium by biomimetic deposition. The CaP coatings show an amorphous and poorly crystallized phase structure and the Ca/P ratio is in the range of 0.89~1.31. The amount and size of cracks in the coatings decrease with increasing Ca and P ion concentration. The Ca-P coating has tailored the corrosion of the magnesium substrate. The corrosion resistance of ZK60 alloy is obviously improved after coated with CaP coatings and the sample with CaP coating deposited from the 2xR-SBF solution has the best corrosion resistance. The improvement in corrosion resistance will greatly reduce the initial biodegradation rate of the implants, and is essential for maintaining the implant's mechanical strength in the bone reunion period. Thus ZK60 alloy coated with the Ca-P coating prepared in this study is a promising candidate for biodegradable orthopedic implant.

ACKNOWLEDGEMENTS

The present work was supported by National Natural Science Foundation of China (Grant No. 50901052) and Program for Young Excellent Talents in Tongji University (Grant No. 2009KJ003) and "Chen Guang" project (Grant No.10CG21) supported by Shanghai Municipal Education Commission and Shanghai Education Development Foundation.

References

1. Mark P. Staiger, Alexis M. Pietak, Jerawala Huadmai, George Dias. *Biomaterials*, 27 (2006) 1728–

1734

2. Frank Witte, Norbert Hort, Carla Vogt, Smadar Cohen, Karl Ulrich Kainer, Regine Willumeit, Frank Feyerabend. *Current Opinion in Solid State and Materials Science*, 12 (2008) 63–72
3. J.Y. Wang, B.H. Wicklund, R.B. Gustilo, D.T. Tsukayama, *Biomaterials*, 17 (1996) 2233–2240
4. Y.W. Song, D.Y. Shan, E.H. Han, *Materials Letters*, 62 (2008) 3276–3279
5. G. Song, S. Song, *Advanced Engineering Materials*, 9 (2007) 298–302
6. A. Feng, Y. Han, The microstructure, *Journal of Alloys and Compounds*, 504 (2010) 585–593
7. A.M. Fekry, R.H. Tammam, *Int. J. Electrochem. Sci.*, 7 (2012) 12254 – 12261
8. D.A. Robinson, R.W. Griffith, D. Shechtman, R.B. Evans, M.G. Conzemius, *Acta Biomaterialia*, 6 (2010) 1869–1877
9. El-Sayed M. Sherif. *Int. J. Electrochem. Sci.*, 7 (2012) 4235 – 4249
10. El-Sayed M. Sherif. *Int. J. Electrochem. Sci.*, 7 (2012) 5084 – 5099
11. El-Sayed M. Sherif, Abdulhakim A. Almajid. *Int. J. Electrochem. Sci.*, 6 (2011) 2131– 2148
12. S.M.M. Shanab, M. A. Ameer, A. M. Fekry, A. A. Ghoneim, and E. A. Shalaby. *Int. J. Electrochem. Sci.*, 6 (2011) 3017 – 3035
13. Zhan Yu, Dongying Ju, Hongyang Zhao. *Int. J. Electrochem. Sci.*, 7 (2012) 7098 – 7110
14. A.M. Fekry and M.A. Ameer. *Int. J. Electrochem. Sci.*, 6 (2011) 1342 – 1354
15. Khalil Abdelrazek Khalil, El-Sayed M. Sherif, Abdulhakim A. Almajid. *Int. J. Electrochem. Sci.*, 6 (2011) 6184 – 6199
16. W. Zhang, B. Tian, K. Q. Du, H. X. Zhang, F. H. Wang. *Int. J. Electrochem. Sci.*, 6 (2011) 5228–5248
17. Shanna Xu, Magdalene Edet Ikpi, Junhua Dong, Jie Wei, Wei Ke, Nan Chen. *Int. J. Electrochem. Sci.*, 7 (2012) 4735 – 4755
18. Ning Ma, Qiuming Peng, Xuejun Li, Hui Li, Jinghuai Zhang, Yongjun Tian. *Int. J. Electrochem. Sci.*, 7 (2012) 8020 - 8034
19. Hui Du, Zunjie Wei, Xinwang Liu, Erlin Zhang. *Materials Chemistry and Physics*, 125 (2011) 568–575
20. Qiuming Peng, Shuangshuang Zhao, Hui Li, Ning Ma, Xuejun Li, Yongjun Tian. *Int. J. Electrochem. Sci.*, 7 (2012) 5581 – 5595
21. Xiaobo Zhang, Guangyin Yuan, Lin Mao, Jialin Niu, Penghuai Fu, Wenjiang Ding. *J. Mech. Behav. Biomed. Mater.*, 7 (2012) 77-86
22. A. R. Shashikala, R. Umarani, S. M. Mayanna and A. K. Sharma. *Int. J. Electrochem. Sci.*, 3 (2008) 993 – 1004
23. Jothi Sudagar, Guangli Bi, Zhonghao Jiang, Guangyu Li, Qing Jiang, Jianshe Lian. *Int. J. Electrochem. Sci.*, 6 (2011) 2767 – 2788
24. Jingxin Yang, Fuzhuai Cui, and In Seop Lee. *Annals of Biomedical Engineering*, 39, (2011) 1857–1871
25. Lei Li, Qing Qu, Zhiwen Fang, Lin Wang, Yunwei He, Rui Yuan, Zhongtao Ding, *Int. J. Electrochem. Sci.*, 7 (2012) 12690 – 12705
26. Yingchao Su, Guangyu Li, Jianshe Lian. *Int. J. Electrochem. Sci.*, 7 (2012) 11497 – 11511
27. Pamela Habibovic, Florence Barre`re, Clemens A. van Blitterswijk, Klaas de Groot, and Pierre Layrolle. *J. Am. Ceram. Soc.*, 85 (2002) 517–22
28. Tal Reiner, Leonid M. Klinger, and Irena Gotman. *Crystal Growth & Design*, 11 (2011) 190–195
29. Shaylin Shadanbaz, George J. Dias. *Acta Biomaterialia*, 8 (2012) 20–30
30. LI KaiKai, WANG Bing, YAN Biao & LU Wei. *Chin. Sci. Bull.*, 57 (2012) 2319~2322
31. A. L. Oliveira, A. J. Pedro, C. Saiz Arroyo, J. F. Mano, G. Rodriguez, J. San Roman, R. L. Reis. *Journal of Biomedical Materials Research Part B: Applied Biomaterials*, 92 (2010) 55–67
32. F. Yang, J.G.C. Wolke, J.A. Jansen. *Chemical Engineering Journal*, 137 (2008) 154–161
33. Ahmet Pasinli, Mithat Yuksel, Erdal Celik, Sevil Sener, A. Cuneyt Tas. *Acta Biomaterialia*, 6 (2010) 2282–2288

34. Wei Lu, Zhe Chen, Ping Huang and Biao Yan. *Int. J. Electrochem. Sci.*, 7 (2012) 12668 – 12679
35. F. Barrere, C.A van Blitterswijk, K. de Groot, P. Layrolle. *Biomaterials*, 23 (2002) 2211–2220
36. Daniel O. Costa, Bedilu A. Allo, Robert Klassen, Jeffrey L. Hutter, S. Jeffrey Dixon, and Amin S. Rizkalla. *Langmuir*, 28 (2012) 3871–3880
37. X. Lu, Y. Leng. *Biomaterials*, 26 (2005) 1097–1108.
38. F. Barrere, *Biomimetic Calcium Phosphate Coatings: Physicochemistry and Biological Activity*, University of Twente, Enschede, 2002
39. A. Bigi, G. Falini, E. Foresti, A. Ripamonti, M. Gazzano, N. Roveri, *Journal of Inorganic Biochemistry*, 49 (1993) 69–78.
40. A. Oyane, Y. Ishikawa, A. Yamazaki, Y. Sogo, K. Furukawa, T. Ushida, A. Ito. *Acta Biomater.*, 4 (2008) 1342–1348
41. R. G. Guan, I. Johnson, T. Cui, T. Zhao, Z. Y. Zhao, X. Li, H. Liu, *J. Biomed Mater Res A.*, 100 (2012) 999-1015
42. A. Atrens, M. Liu, N. I. Z.I Abidin, *Materials Science and Engineering B*, 176 (2011) 1609-1636